GEOPHYSICS, VOL. 63, NO. 5 (SEPTEMBER-OCTOBER 1998); P. 1652–1658, 11 FIGS., 1 TABLE.

Effects of attenuation and anisotropy on reflection amplitude versus offset

José M. Carcione*, Hans B. Helle‡, and Tong Zhao**

ABSTRACT

To investigate the effects that attenuation and anisotropy have on reflection coefficients, we consider a homogeneous and viscoelastic wave incident on an interface between two transversely isotropic and lossy media with the symmetry axis perpendicular to the interface. Analysis of PP and PS reflection coefficients shows that anisotropy should be taken into account in amplitude variation with offset (AVO) studies involving shales. Different anisotropic characteristics may reverse the reflection trend and substantially influence the position of the critical angle versus offset. The analysis of a shale-chalk interface indicates that when the critical distance is close to the near offsets, the AVO response is substantially affected by the presence of dissipation. In a second example, we compute reflection coefficients and synthetic seismograms for a limestone/black shale interface with different rheological properties of the underlying shale. This case shows reversal of the reflection trend with increasing offset and compensation between the anisotropic and anelastic effects.

INTRODUCTION

Rock characterization from seismic data is a challenging task that requires a proper description of the constitutive equation. At present, processing and inversion algorithms assume simplified rheologies and are based mainly on traveltime information that gives a rough estimation of the compressional wave velocity. However, this property and the underlying simplifications are not appropriate for characterizing the rock. Additional valuable information contained in the data are the effects produced by rock symmetry (anisotropy) and relaxation mechanisms (attenuation) (Arts, 1993; Yin, 1993). In particular, quality factor (Q) is a better indicator of fluid content than wave velocity, and Q anisotropy is a better indicator of material symmetry than velocity anisotropy (Carcione and Cavallini, 1995).

While the use of realistic rheologies in inversion techniques is a difficult task (owing to the number of material properties), the use of AVO methods could be more suitable for rock characterization. Some work has been done in this direction. For instance, Bourbie (1982, 1984) and Samec and Blangy (1992) show an amplitude jump in the AVO trend, caused by anelasticity. On the other hand a number of studies consider anisotropy, e.g., Wright (1987), Graebner (1992), Kim et al. (1993), and Blangy (1994).

Since attenuation is attributed to a large variety of dissipation mechanisms, it is difficult—if not impossible—to build a general microstructure theory embracing all these mechanisms. A dissipation model consistent with rock properties is the general standard linear solid. This is based on a spectrum of relaxation mechanisms and is suitable for wavefield computations in the time domain. One relaxation function describes the anelastic properties of the quasi-dilatational mode, and the other three model the anelastic properties of the shear modes.

As mentioned before, the analysis of the effects that the different rock properties have on the seismic response is crucial for a proper characterization of the medium. Analysis of the reflection coefficients versus propagation angle provides further insight into the influence of these properties on the AVO signature. In the first part of this work, we briefly describe the reflection-transmission problem between two viscoelastic transversely isotropic (VTI) media with the symmetry axes perpendicular to the interface. Then we consider the elastic models studied by Wright (1987), extending the analysis to the viscoelastic case. Finally, we investigate the AVO response of a kerogen-rich shale (Vernik and Nur, 1992) overlaid by an elastic and isotropic limestone.

Manuscript received by the Editor August 19, 1996; revised manuscript received December 10, 1997.
*Osservatorio Geofisico Sperimentale, P.O. Box 2011, Opicina, 34016 Trieste, Italy; E-mail: jcarcione@ogs.trieste.it.
‡Norsk Hydro a.s., E&P Research Centre, N-5020 Bergen, Norway; E-mail: hans.b.helle@nho.hydro.com.
**China National Petroleum Corporation, Synthesis Division, Exploration Bureau, P.O. Box 766, Liu Pu Kang, Beijing 100724, China; E-mail: zhao@mail.cnpc.co.cn.

CONSTITUTIVE EQUATION AND *Q*-ANISOTROPY

The theory assigns one dissipation mechanism to each fundamental deformation of the medium. The convention is to denote the quasi-dilatational and quasi-shear deformations with ($\nu = 1$) and ($\nu = 2$), respectively.

The complex stiffnesses relating stress and strain are (Carcione, 1995, 1997)

$$p_{11} = c_{11} - D + KM_1 + c_{55}M_2, \tag{1}$$

$$p_{33} = c_{33} - D + KM_1 + c_{55}M_2, \tag{2}$$

$$p_{13} = c_{13} - D + KM_1 + c_{55}(2 - M_2), \tag{3}$$

and

$$p_{55} = c_{55}M_2. \tag{4}$$

The elastic constants c_{IJ}, $I, J = 1, \ldots, 6$ are the unrelaxed or high-frequency limit stiffnesses. Moreover,

$$K = D - c_{55}, \qquad D = \tfrac{1}{2}(c_{11} + c_{33}) \tag{5}$$

and

$$M_\nu = \frac{\tau_\sigma^{(\nu)}}{\tau_\epsilon^{(\nu)}}\left(\frac{1 + i\omega\tau_\epsilon^{(\nu)}}{1 + i\omega\tau_\sigma^{(\nu)}}\right), \qquad \nu = 1, 2 \tag{6}$$

are Zener complex moduli, where

$$\tau_\epsilon^{(\nu)} = \frac{\tau_0}{Q_\nu}\left[\sqrt{Q_\nu^2 + 1} + 1\right] \tag{7}$$

and

$$\tau_\sigma^{(\nu)} = \frac{\tau_0}{Q_\nu}\left[\sqrt{Q_\nu^2 + 1} - 1\right], \tag{8}$$

with τ_0 a relaxation time such that $1/\tau_0$ is the center angular frequency of the relaxation peak and $1/Q_\nu$ is the maximum quality factor. Note that Q_1 and Q_2 are single-value parameters quantifying the attenuation of the fundamental deformation modes.

The quality factor of the qP- and qS-waves depends on the propagation direction and, of course, the frequency of the signal. They are given by (Carcione and Cavallini, 1995)

$$Q = \frac{\mathrm{Re}(V^2)}{\mathrm{Im}(V^2)}, \tag{9}$$

where Re and Im denote real and imaginary parts, respectively. The complex velocity V can be calculated from

$$\rho V^2 = \tfrac{1}{2}\left(p_{55} + p_{11}\sin^2\theta + p_{33}\cos^2\theta \pm E\right), \tag{10}$$

where θ is the propagation angle, ρ is the density, and

$$E = \left\{\left[(p_{33} - p_{55})\cos^2\theta - (p_{11} - p_{55})\sin^2\theta\right]^2 + (p_{13} + p_{55})^2\sin^2 2\theta\right\}^{1/2}. \tag{11}$$

The plus sign corresponds to the qP-wave, and the minus sign corresponds to the qS-wave.

For qP-waves propagating along the symmetry axis ($\theta = 0$), $\rho V^2 = p_{33}$; in the isotropy plane ($\theta = \pi/2$), $\rho V^2 = p_{11}$. Then the relation between Q factors is

$$\frac{Q(\text{symmetry axis})}{Q(\text{isotropy plane})} = \frac{c_{33} - A}{c_{11} - A}, \qquad A = D - K\,\mathrm{Re}(M_1) - G\,\mathrm{Re}(M_2). \tag{12}$$

The ratio between the viscoelastic phase velocities $\mathrm{Re}(1/\sqrt{p_{11}})/\mathrm{Re}(1/\sqrt{p_{33}})$ is closer to one than the Q ratio. When $c_{11} > c_{33}$ (e.g., fine layering), the qP-wave attenuates more along the symmetry axis than in the plane of isotropy. It is not necessary to use an additional relaxation function to model Q anisotropy of the qP-wave. Actually, the structure of the medium (described by the stiffnesses) dictates the Q ratio between different propagation directions. On the other hand, the quality factor of the shear wave at the symmetry axis is equal to the quality factor in the plane of isotropy, since $V^2 = \rho p_{55}$ in both cases.

REFLECTION-TRANSMISSION PROBLEM

The problem of reflection and refraction at an interface between two anelastic transversely isotropic media whose respective symmetry axes are perpendicular to the interface has been investigated by Carcione (1997). He considered a homogeneous incident wave and obtained the attributes of the reflected and transmitted waves such as, for instance, the energy reflection coefficients, the phase and energy velocities, the quality factor, and the interference coefficients.

A general solution for the particle velocity field $\underline{\mathbf{v}} = (v_x, v_z)$ is

$$\underline{\mathbf{v}} = i\omega\underline{\mathbf{U}}\exp[i\omega(t - s_x x - s_z z)], \tag{13}$$

where s_x and s_z are the components of the complex slowness vector, t is the time variable, and $\underline{\mathbf{U}}$ is a complex displacement vector.

For homogeneous waves the directions of propagation and attenuation coincide and

$$s_x = \sin\theta/V(\theta), \qquad s_z = \cos\theta/V(\theta), \tag{14}$$

where θ is the propagation angle, measured with respect to the z-axis, and V is given in equation (10).

Let us assume that the positive z-axis points downward. To distinguish between downward and upward propagating waves, the slowness relation is solved for s_z, given the horizontal slowness s_x. It yields

$$s_z = \pm\frac{1}{\sqrt{2}}\left(K_1 \mp p.v.\sqrt{K_1^2 - 4K_2K_3}\right)^{1/2}, \tag{15}$$

In equation (15),

$$K_1 = \rho\left(\frac{1}{p_{55}} + \frac{1}{p_{33}}\right) + \frac{1}{p_{55}}\left[\frac{p_{13}}{p_{33}}(p_{13} + 2p_{55}) - p_{11}\right]s_x^2,$$

$$K_2 = \frac{1}{p_{33}}\left(p_{11}s_x^2 - \rho\right),$$

and

$$K_3 = s_x^2 - \frac{\rho}{p_{55}}.$$

The value $p.v.(z)^{1/2}$ denotes the principal value of the square root of the complex number z. The signs corresponds to

$$(+,-) \quad \text{downward } qP\text{-wave},$$
$$(+,+) \quad \text{downward } qS\text{-wave},$$
$$(-,-) \quad \text{upward } qP\text{-wave, and}$$
$$(-,+) \quad \text{upward } qS\text{-wave}.$$

Application of welded boundary conditions generates the following matrix equation for the reflection and transmission coefficients R and T:

$$\begin{pmatrix} \beta_{P_1} & \beta_{S_1} & -\beta_{P_2} & -\beta_{S_2} \\ \gamma_{P_1} & \gamma_{S_1} & \gamma_{P_2} & \gamma_{S_2} \\ Z_{P_1} & Z_{S_1} & -Z_{P_2} & -Z_{S_2} \\ W_{P_1} & W_{S_1} & W_{P_2} & W_{S_2} \end{pmatrix} \begin{pmatrix} R_{PP} \\ R_{PS} \\ T_{PP} \\ T_{PS} \end{pmatrix} = \begin{pmatrix} -\beta_{P_1} \\ \gamma_{P_1} \\ -Z_{P_1} \\ W_{P_1} \end{pmatrix}. \tag{16}$$

The quantities β and γ are the horizontal and vertical complex polarizations, respectively, given by

$$\beta = p.v.\left[\frac{p_{55}s_x^2 + p_{33}s_z^2 - \rho}{p_{11}s_x^2 + p_{33}s_z^2 + p_{55}(s_x^2 + s_z^2) - 2\rho}\right]^{1/2} \tag{17}$$

and

$$\gamma = \pm p.v.\left[\frac{p_{11}s_x^2 + p_{55}s_z^2 - \rho}{p_{11}s_x^2 + p_{33}s_z^2 + p_{55}(s_x^2 + s_z^2) - 2\rho}\right]^{1/2}, \tag{18}$$

where the plus and minus signs correspond to the qP- and qS-waves, respectively. Then,

$$W = p_{55}(\gamma s_x + \beta s_z) \tag{19}$$

and

$$Z = \beta p_{13} s_x + \gamma p_{33} s_z. \tag{20}$$

The upper layer is denoted by the subscript 1 and the lower layer by the subscript 2. The symbols P and S indicate the qP- and qS-waves, respectively.

EXAMPLES

The material properties of the different rocks are given in Table 1, where $V_{IJ} = \sqrt{c_{IJ}/\rho}$ and δ and ϵ denote the anisotropic coefficients introduced by Thomsen (1986). The first example considers three models of anisotropic and dissipative shales overlying an isotropic and elastic chalk. The unrelaxed velocities of the shales are indicated in the table. Wright (1987) calculates the reflection coefficient for the elastic case, which is equivalent to the high-frequency limit. The comparison between the absolute values of the elastic and anelastic R_{PP} is shown in Figures 1 and 2 for $Q_1 = 100$, $Q_2 = 80$ and $Q_1 = 20$, $Q_2 = 15$, respectively. In both cases, Q anisotropy [relation (12)] in the shales is approximately 0.6, whereas velocity anisotropy is 0.8. Figures 1 and 2 show that the main differences between the elastic and the anelastic cases occur near the critical angle and beyond it. These differences are substantial in Figure 2, affecting also the reflection coefficient at near offsets when the overlying medium is shale 1. At zero offset, the elastic and anelastic cases yield similar results, in agreement with Bourbie (1984). Figures 3 and 4 represent the phase behavior of the reflection coefficients R_{PP} for weak and strong attenuation, respectively. As can be seen, the phase differences are important for ray angles close to the critical angle, where they reach a maximum value.

The combined effect of anisotropy and dissipation on the reflection coefficient can be appreciated in Figure 5, where the curves correspond to an isotropic and elastic overlying shale and to the overlying anisotropic shale 1 in Table 1, assuming weak, strong, and no losses. The isotropic shale is obtained by making $V_{11} = V_{33}$ and $V_{13} = 2514$ m/s. The picture shows that the assumption of an ideal (elastic and isotropic) rheological equation can be applied only to the very near offsets, and that AVO analysis requires the use of a more realistic constitutive relation.

In the second example we analyze the reflection coefficient between a source-rock shale and an elastic and isotropic limestone (see Table 1). The aim is to investigate if seismic detection of organic-rich shales can be feasible for AVO techniques, taking into account the anisotropic properties of these rocks (Vernik and Landis, 1996). The anisotropy is related to the kerogen content and can be further enhanced by the effect of temperature and pressure. In fact, Figure 6 represents Thomsen's anisotropic parameters (including γ) versus kerogen content for the North Sea Kimmeridgian shale (Vernik, 1995). A linear fit of the experimental data shows that the shale is substantially anisotropic, with positive ϵ and γ, which is a characteristic of laminar transversely isotropic composites. The positive and negative δ values indicate that the wavefront radius of curvature may present large variations. Since Thomsen's parameters are zero for the overlying isotropic limestone, the anisotropic behavior of the P-wave reflection coefficient is determined solely by the shale parameters; δ dominates at near offsets, and ϵ influences the response at large incidence angles (Kim et al., 1993; Rueger, 1995).

We consider the black shale 1 given in Table 1 and its isotropic version (black shale 2). Figure 7 represents the group velocity of the quasi-compressional wave for both media. The high attenuation level of the first example is assumed, i.e., we compare reflection coefficients and phases for underlying shales with strong and no losses (Figures 8 and 9). The reflection coefficient of the isotropic shale increases with offset,

Table 1. Material properties.

Rock	V_{11} (m/s)	V_{33} (m/s)	V_{55} (m/s)	V_{13} (m/s)	δ	ϵ	ρ (g/cm^3)
Shale 1	3810	3048	1219	609	−0.40	0.28	2.3
Shale 2	3810	3048	1402	1828	−0.26	0.28	2.3
Shale 3	3810	3048	1402	3048	0.38	0.28	2.3
Chalk	5029	5029	2621	3414	≈0.00	0.00	2.7
Limestone	3340	3340	1300	2788	0.00	0.00	2.7
Black shale 1	3590	2650	1300	2443	0.40	0.42	2.7
Black shale 2	2650	2650	1300	1909	0.00	0.00	2.7

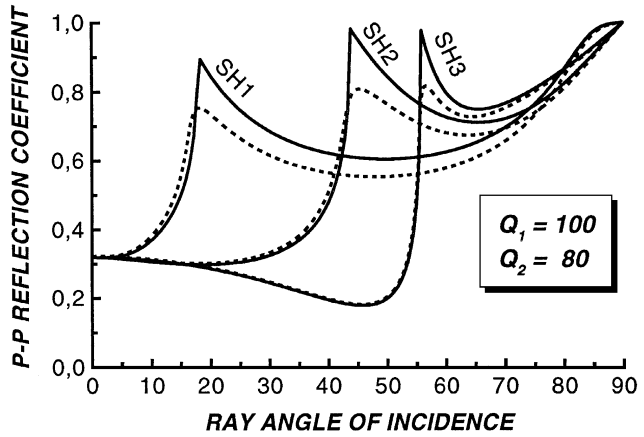

FIG. 1. Absolute value of the *P*-wave reflection coefficient versus ray angle for three different lossy and anisotropic shales overlying an isotropic and elastic chalk. The purely elastic case, analyzed by Wright (1987), is represented by a continuous line. The unrelaxed velocities and density of the different rocks are given in Table 1, and the dissipation parameters for the shales are $Q_1 = 100$ and $Q_2 = 80$ (weak loss).

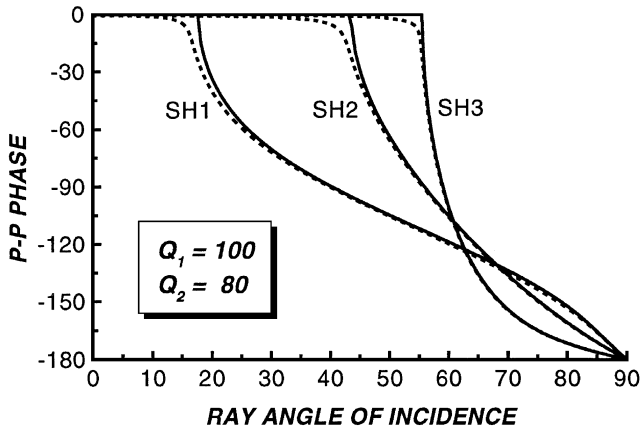

FIG. 3. Phase angle of the *P*-wave reflection coefficient versus ray angle corresponding to the case illustrated in Figure 1. The elastic case is represented by a continuous line.

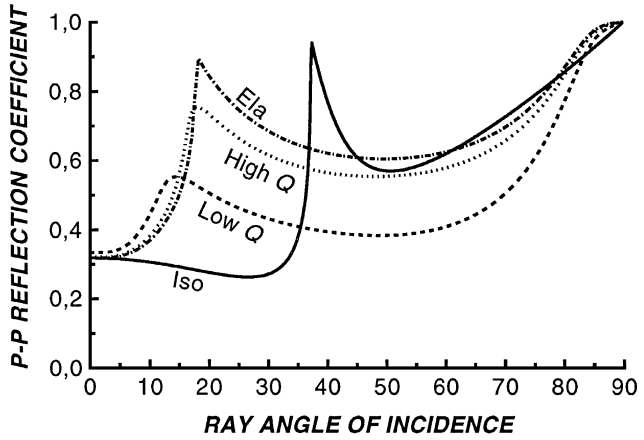

FIG. 5. Comparison between the purely elastic and isotropic reflection coefficient (continuous line) and the reflection coefficients corresponding to shale 1 with weak (high *Q*), strong (low *Q*), and no losses (Ela).

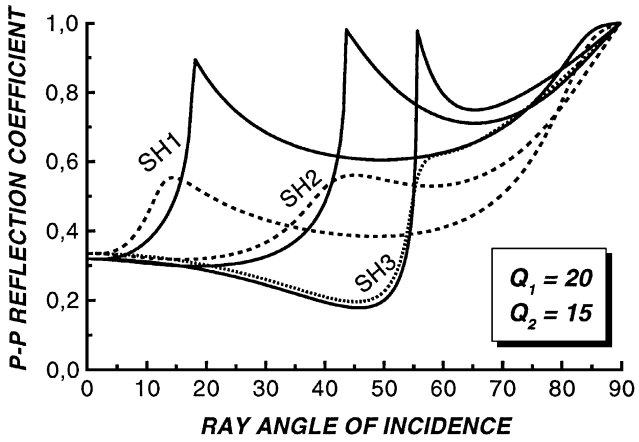

FIG. 2. As in Figure 1, with the dissipation parameters for the shales $Q_1 = 20$ and $Q_2 = 15$ (strong loss).

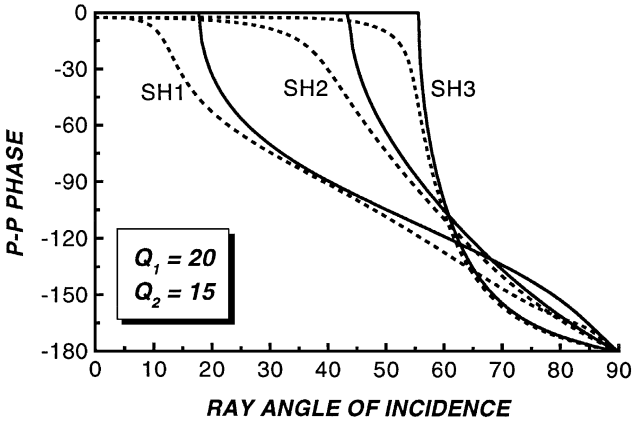

FIG. 4. Phase angle of the *P*-wave reflection coefficient versus ray angle corresponding to the case illustrated in Figure 2. The elastic case is represented by a continuous line.

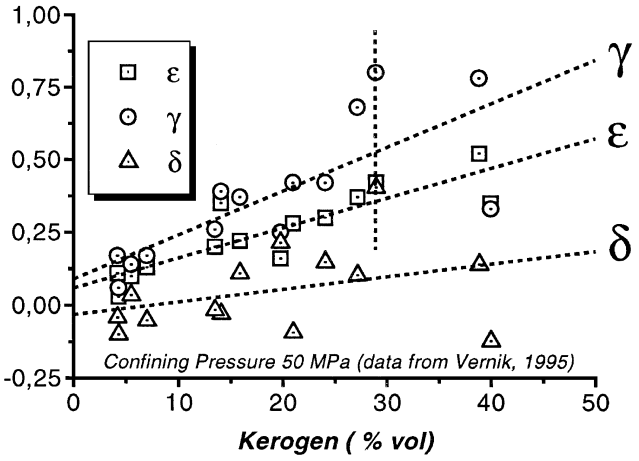

FIG. 6. Thomsen's anisotropic parameters versus kerogen content for the North Sea Kimmeridgian shale. A linear fit of the experimental data shows that the shale is substantially anisotropic. The marked sample is used for computing the reflection coefficients and synthetic seismograms shown in the next figures. (Data from Vernik, 1995.)

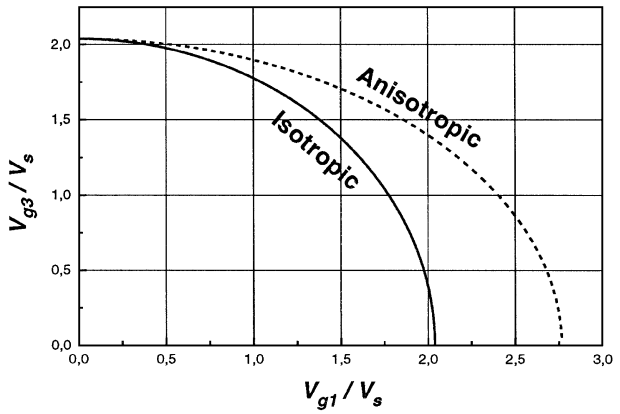

FIG. 7. Normalized group velocity of the quasi-compressional wave corresponding to the black shales (no losses) in Table 1. The broken line corresponds to black shale 1, the continuous line to black shale 2. The normalization factor is the vertical shear velocity.

while that of the anisotropic shale decreases. The presence of dissipation tends to compensate for the anisotropic effect. This reversal in the trend of the reflection coefficient is observed when the P-wave velocity of the upper medium is less than the horizontal P-wave velocity of the lower medium and greater than the respective vertical velocity.

Finally, Figures 10 and 11 show the synthetic seismograms of the particle velocity component v_z corresponding to the various combination of rock properties as represented in Figures 8 and 9. The numerical simulation has been performed by using a wave modeling algorithm based on the Fourier method for computing the spatial derivatives and a fourth-order Runge-Kutta technique for computing the wavefield recursively in time (Carcione, 1995). The source is isotropic in the mean stress $\sigma_{xx} + \sigma_{zz}$ (i.e., an explosion), and its time history is a Ricker-type wavelet with a central frequency of 30 Hz. Since the limestone is isotropic and lossless, the only propagation effects are the geometrical spreading and the particle velocity radiation pattern, which must be considered for comparison with the reflection coefficients. The PS reflection can be seen clearly in the anisotropic synthetics, in agreement with the plane-wave

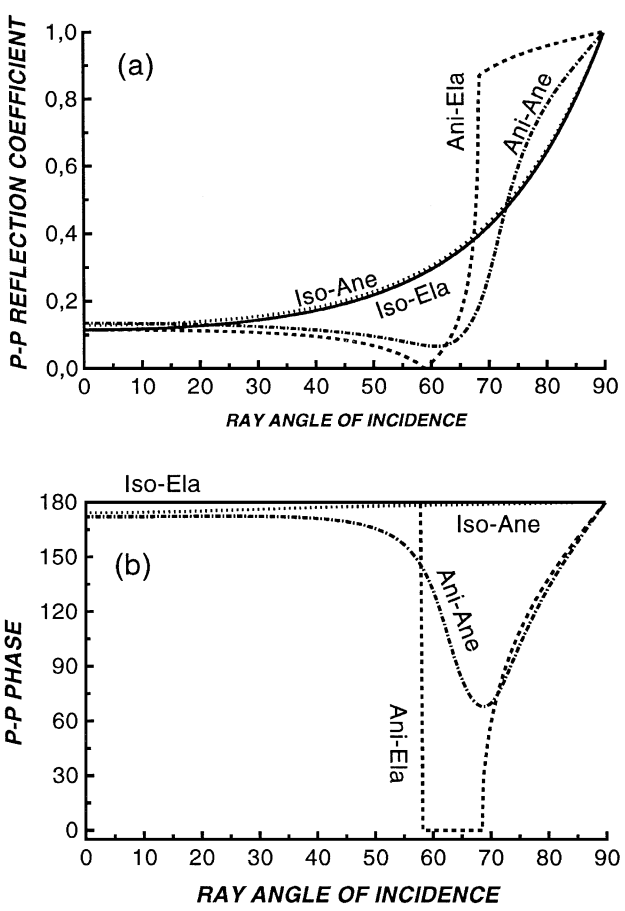

FIG. 8. Absolute value of the P-wave reflection coefficient (a) and phase angle (b) versus ray angle for black shales underlying an isotropic limestone (see properties in Table 1). The high-loss isotropic-anelastic (Iso-Ane) and anisotropic-anelastic (Ani-Ane) and purely elastic cases (Iso-Ela and Ani-Ela) are compared.

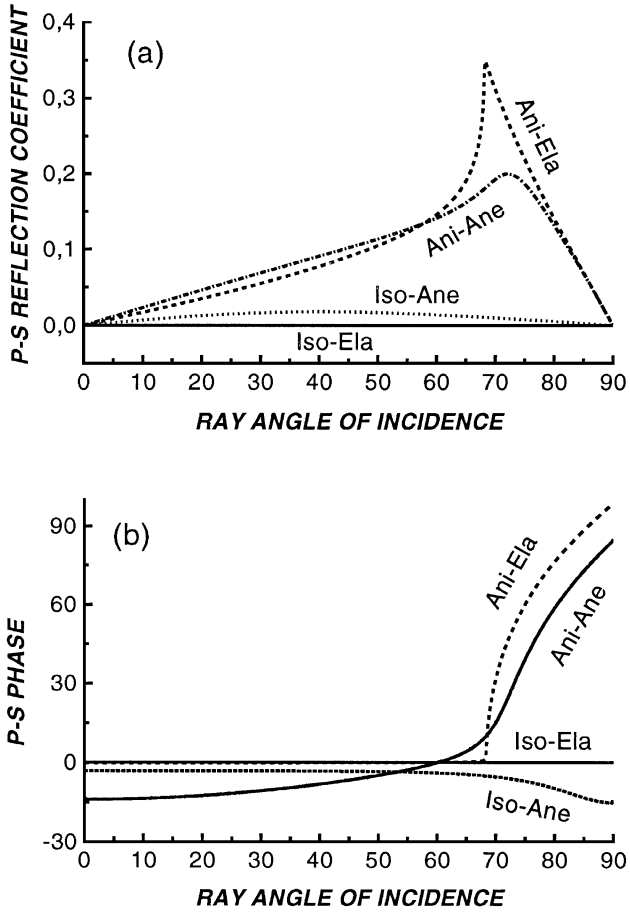

FIG. 9. Absolute value of the PS reflection coefficient (a) and phase angle (b) versus ray angle for black shales underlying an isotropic limestone (see properties in Table 1). The high-loss isotropic-anelastic (Iso-Ane) and anisotropic-anelastic (Ani-Ane) and purely elastic cases (Iso-Ela and Ani-Ela) are compared.

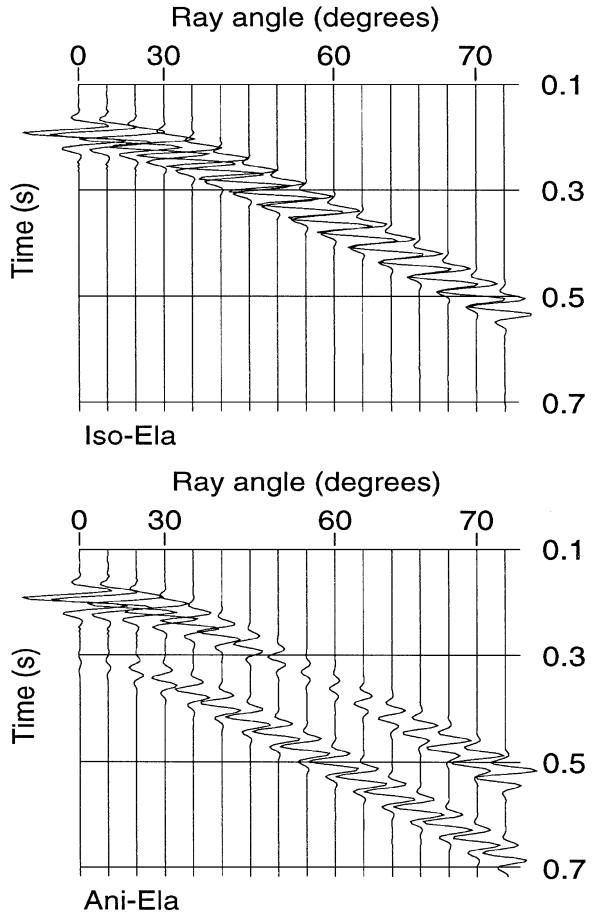

FIG. 10. Synthetic seismograms of the particle velocity component v_z, corresponding to isotropic-elastic (Iso-Ela) and anisotropic-elastic (Ani-Ela) cases represented in Figures 8 and 9. In the Ani-Ela case, note the phase reversal of the *P*-wave reflection near the critical ray angle (≈60°) in accordance with the analytical results shown in Figures 8 and 9.

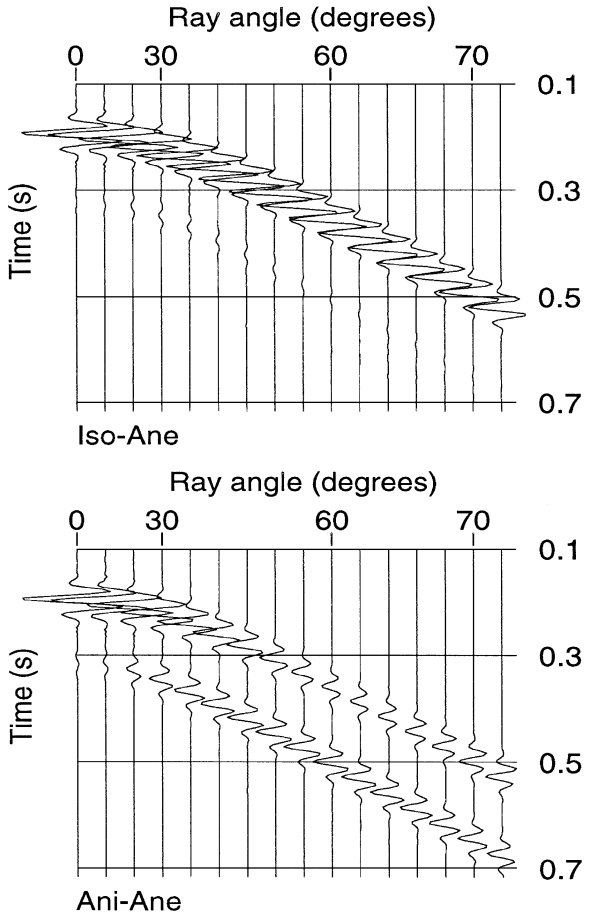

FIG. 11. Synthetic seismograms of the particle velocity component v_z, corresponding to isotropic-anelastic (Iso-Ane) and anisotropic-anelastic (Ani-Ane) cases represented in Figures 8 and 9. In the Ani-Ane case, note a smooth phase transition of the *P*-wave reflection near the critical ray angle (≈60°) in accordance with the analytical results shown in Figures 8 and 9.

analysis. Moreover, the results show the dissimilar behavior of the reflection events at large offsets. The differences are mainly caused by the presence of anisotropy, since, as can be appreciated in Figures 8 and 9, dissipation has less effect on the reflection coefficient.

CONCLUSIONS

The analysis shows that the presence of attenuation affects the *P*-wave reflection coefficient near the critical angle and beyond it. For relatively low *Q*, e.g., sediments and reservoir rocks, these differences are substantial. Moreover, if the critical distance occurs at the near offsets, the presence of attenuation may greatly affect the AVO response. In general, the combined effect of attenuation and anisotropy affects the reflection coefficients at nonnormal incidence.

Theoretical and numerical modeling of a limestone/black shale interface reveals that the presence of anisotropy reverses the trend of the reflection coefficient versus offset and, for this particular case, dissipation tends to compensate the anisotropic effects.

Generally, for subcritical reflections, anisotropic effects are dominant over attenuation effects. However, a more realistic analysis should consider incident inhomogeneous waves, for which equiphase planes are not coincident with equiamplitude planes. These waves are generated at inhomogeneities and interfaces and may considerably affect the reflection coefficient.

ACKNOWLEDGMENTS

We thank Norsk Hydro for financing the research and for permission to publish this paper.

REFERENCES

Arts, R. J., 1993, A study of general anisotropic elasticity in rocks by wave propagation, theoretical and experimental aspects: Ph.D. thesis, Paris Univ.

Blangy, J. P., 1994, AVO in transversely isotropic media—An overview: Geophysics, **59**, 775–781.

Bourbie, T., 1982, The effect of attenuation on reflections: Ph.D. thesis, Stanford Univ.

———1984, Effects of attenuation on reflections: Experimental test: J. Geophys. Res., **89**, 6197–6202.

Carcione, J. M., 1995, Constitutive model and wave equations for linear, viscoelastic, anisotropic media: Geophysics, **60**, 537–548.

———1997, Reflection and refraction of *qP*-*qS* plane waves at a plane boundary between viscoelastic transversely isotropic media: Geophys. J. Internat., **129**, 669–680.

Carcione, J. M., and Cavallini, F., 1995, Attenuation and quality factor surfaces in anisotropic-viscoelastic media: Mechanics of Materials, **19**, 311–327.

Graebner, M., 1992, Plane-wave reflection and transmission coefficients for a transversely isotropic solid: Geophysics, **57**, 1512–1519.
Kim, K. Y., Wrolstad, K. H., and Aminzadeh, F., 1993, Effects of transverse isotropy on *P*-wave AVO for gas sands: Geophysics, **58**, 883–888.
Rueger, A., 1995, *P*-wave reflection coefficients for transversely isotropic media with vertical and horizontal axis symmetry: 65th Ann. Internat. Mtg., Soc. Expl. Geophys., Expanded Abstracts, 278–281.
Samec, P., and Blangy, J. P., 1992, Viscoelastic attenuation, anisotropy and AVO: Geophysics, **57**, 441–450.
Thomsen, L., 1986, Weak elastic anisotropy: Geophysics, **51**, 1954–1966.
Vernik, L., 1995, Petrophysics of the Kimmeridge shale, North Sea: Stanford Rocks Physics Laboratory report.
Vernik, L., and Landis, C., 1996, Elastic anisotropy of source rocks: Implications for hydrocarbon generation and primary migration: AAPG Bulletin, **80**, 531–544.
Vernik, L., and Nur, A., 1992, Ultrasonic velocity and anisotropy of hydrocarbon source-rocks: Geophysics, **57**, 727–735.
Wright, J., 1987, The effects of transverse isotropy on reflection amplitude versus offset: Geophysics, **52**, 564–567.
Yin, H., 1993, Acoustic velocity and attenuation of rocks: Isotropy, intrinsic anisotropy, and stress induced anisotropy: Ph.D. thesis, Stanford Univ.